

Impact of chaos on precursors of quantum criticality

Ignacio García-Mata,¹ Eduardo Vergini,² and Diego A. Wisniacki³

¹*Instituto de Investigaciones Físicas de Mar del Plata (IFIMAR), Facultad de Ciencias Exactas y Naturales, Universidad Nacional de Mar del Plata and CONICET, 7600 Mar del Plata, Argentina*

²*Departamento de Física, Comisión Nacional de Energía Atómica.,
Avenida del Libertador 8250, (C1429BNP) Buenos Aires, Argentina
Escuela de Ciencia y Tecnología, Universidad Nacional de General San Martín,
Alem 3901, (B1653HIM) Villa Ballester, Argentina*

³*Departamento de Física “J. J. Giambiagi” and IFIBA, FCEyN, Universidad de Buenos Aires, 1428 Buenos Aires, Argentina
(Dated: December 28, 2021)*

Excited-state quantum phase transitions (ESQPTs) are critical phenomena that generate singularities in the spectrum of quantum systems. For systems with a classical counterpart, these phenomena have their origin in the classical limit when the separatrix of an unstable periodic orbit divides phase space into different regions. Using a semiclassical theory of wave propagation based on the manifolds of unstable periodic orbits, we describe the quantum states associated with an ESQPT for the quantum standard map: a paradigmatic example of a kicked quantum system. Moreover, we show that finite-size precursors of ESQPTs shrink as chaos increases due to the disturbance of the system. This phenomenon is explained through destructive interference between principal homoclinic orbits.

Critical phenomena are ubiquitous in physics. They are characterized by non-analyticities of measurable observables and have a profound impact on several aspects of the statistical and dynamical properties of physical systems [1]. In quantum mechanics, criticality can manifest itself in individual states due to the discreteness of the spectrum. For instance, at zero temperature, a quantum phase transition is expressed by an abrupt change in the ground state when a parameter is varied [2]. When this occurs for excited states, it is called excited-state quantum phase transition (ESQPT) [3]. It appears when the level density reveals singularities that have important consequences in the collective behavior of interacting many-body systems [3]. It also has effects on decoherence [4, 5], quantum thermodynamics [6, 7], quantum information [8], and condensate physics [9, 10].

ESQPTs have been studied in autonomous and periodically driven systems. In the latter, criticality appears in quasi-energy states, which are a direct generalization of ESQPTs for driven quantum systems [11–13]. The Floquet map represents the collective variables of a many-body system. In general ESQPTs have been related to phase space structures associated with the classical-limit of the system [3]. In classical integrable systems, unstable periodic orbits and their manifolds make up the separatrices that divide classical phase space into disjoint areas of regular motion. Moreover, they are sensitive to disturbances giving rise to chaotic regions when the system is perturbed, that is, their breakdown generates homoclinic and heteroclinic tangles which are the originating causes of chaos [14]. Although some consequences of the destruction of these structures have been studied in connection with ESQPT [3, 15–20], the main aspects of this process have yet to be understood.

Semiclassical theories have been the bridge between the classical and quantum worlds and have had extraordinary success in explaining various phenomena [21]. For

integrable or strongly chaotic motions, semiclassical theories are much more developed [22] than in the case of nearly integrable or mixed dynamics, where islands of stability coexist with chaotic layers [23]. At the same time, ESQPTs have been described using semiclassical torus quantization near a separatrix, but this technique works for integrable systems but fails when chaos appears. In this case the separatrix associated with the unstable periodic orbit (PO) breaks, and new invariant structures which are robust with respect to perturbations emerge; the stable and unstable manifolds. Recently, a semiclassical theory of wave propagation based on stable and unstable manifolds of unstable POs was developed [24–26]. This method has been proven to be very efficient for the calculation of high energy levels of strongly chaotic systems [27], but it has yet to be tested (used) in the mixed regime.

In this Letter we use this state of the art semiclassical method to show that the advent of chaos in the classical model can result in the weakening of finite-size precursors of ESQPTs. We find a simple semiclassical criterion specifying the transition from the finite size manifestation of quantum criticality to quantum chaos. We predict when this effect occurs depending on the size of the disturbance that changes the ratio between a canonical invariant of the principal homoclinic orbits and the Planck constant in our model (or the inverse of the number of particles in many-body systems). The decrease of finite-size precursors of ESQPTs is produced by the interference of principal homoclinic orbits giving rise to scarred states – i.e., states with accumulated probability density – on satellite POs related to the homoclinic motion [28, 29].

For our calculations we have used a map that stems from a periodically kicked Hamiltonian, the paradigmatic standard map [30]. However, it is important to highlight that the conclusions reached have general validity. The standard map is a two-dimensional area-preserving map

depending on a perturbation parameter k . This map evolves a point $z = (q, p)$ in the unit torus to the point $z' = (q', p')$ by the following rule

$$\begin{aligned} p' &= p + \frac{k}{2\pi} \sin(2\pi q), \\ q' &= p' + q \end{aligned} \quad \text{mod } 1 \quad (1)$$

This map is generated by the time-dependent Hamiltonian $H(q, p, t) = p^2/2 + k/(2\pi)^2 \cos(2\pi q) \sum \delta(t-n)$. For small $k \approx 0$ the map is almost integrable, and as k increases, invariant tori begin to break. For very large k there are no visible regular islands (although small ones do appear for certain values); Figure 1 shows phase portraits for $k = 0.001, 0.2, 0.5, 1, 1.5$ and 1.8 . Upon quantization the map is a unitary operator that can be expressed as a product of two kicks,

$$\hat{U} = \exp\left(-i\frac{\hat{p}^2}{2\hbar}\right) \exp\left(-i\frac{k}{\hbar} \cos(2\pi\hat{q})\right). \quad (2)$$

The phase space topology implies a finite Hilbert space of dimension N , and effective Planck constant $\hbar = 1/(2\pi N)$. Therefore, \hat{U} is represented by an $N \times N$ matrix and after diagonalization, we analyze spectral properties in terms of the set of eigenphases ϕ_i corresponding to the eigenstates $\hat{U}|\phi_i\rangle = e^{i\phi_i}|\phi_i\rangle$. We emphasize that the parameter N corresponds to the particle number in a many-body system[11].

We now consider precursors of critical behavior in the quasienergy spectrum associated with the separatrix generated by the unstable PO of period 1 at $z_0 = (0, 0)$. Such an invariant structure is broken even for an arbitrarily small perturbation, and then a chaotic layer dominated by the stable and unstable manifolds of z_0 emerges [see Figs. 1(a)-1(f)]. In order to study eigenfunctions localized on invariant curves influenced by z_0 , we compute $|z_0\rangle = \sum c_i |\phi_i\rangle$, with $|z_0\rangle$ being a suitable normalized wave packet centered at z_0 . This wave packet is the map version of a Gaussian beam construction on unstable POs, named the resonance of the PO [31] (see the Supplemental Material [32]).

In Fig. 1 (central frame) we show the eigenphases as a function of the perturbation k (gray lines) for $N = 158$. The thick colored lines mark eigenstates with high (darker shade) intensity $|c_i|^2$. One clearly sees the emergence of an ESQPT precursor spectral structure, in the form of Demkov-type avoided level crossings[33, 34] that follows the states with the greatest overlap with the resonance of z_0 (darker shade in Fig. 1). This structure follows a straight line which can be identified with the Bohr-Sommerfeld (BS) phase ϕ_{BS} . The BS phase of $|z_0\rangle$ is a semiclassical estimate for the phase of the matrix element $\langle z_0|\hat{U}|z_0\rangle$, resulting in [35]

$$\phi_{BS} = \left(-\frac{kN}{2\pi}\right)_{\text{mod}(2\pi)} \simeq \sum |c_i|^2 \tilde{\phi}_i, \quad (3)$$

and the corresponding phase dispersion is given by $\sigma_\phi = \lambda/\sqrt{2} \simeq [\sum |c_i|^2 (\tilde{\phi}_i - \phi_{BS})^2]^{1/2}$, with

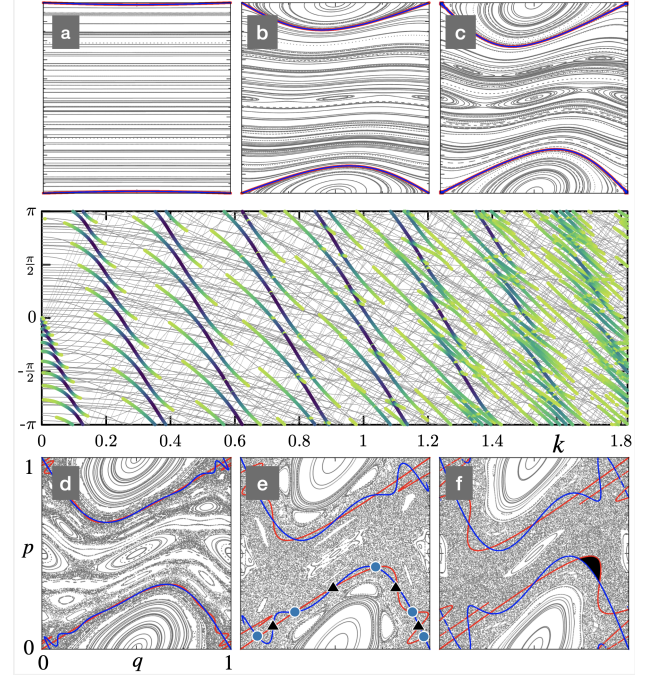


Figure 1. (a-f) Classical phase space for the standard map for $k = 0.001, 0.2, 0.5, 1, 1.5$ and 1.8 , showing the stable (blue line) and unstable (red line) manifolds of z_0 . (e) displays the first (circles) and second (triangles) homoclinic orbits of z_0 . (f) shows a black area indicating the invariant ΔS . The middle panel shows a correlation diagram for the eigenphases of the quantized standard map with $N = 158$ as a function of the perturbation parameter k ; high intensities $|c_i|^2 > 5 \times 10^{-3}$ are plotted in color.

$\lambda = \ln\left(1 + k/2 + \sqrt{k + k^2/4}\right)$ being the stability exponent of z_0 . Here $\tilde{\phi}_i$ is just ϕ_i or $\phi_i \pm 2\pi$; one selects the value that minimizes $(\tilde{\phi}_i - \phi_{BS})^2$. This non-isolated avoided crossing structure is observed in several models of many-body systems [3]. It can also be observed in the elliptic billiard [34] and molecular systems [33, 36]. Figure 1 also shows that as the perturbation grows, this structure gradually disappears, and for $k \gtrsim 1.4$ it is difficult to observe the sequence of Demkov avoided crossings. Understanding the physical process involved in the destruction of this structure is the most important achievement of this Letter. We emphasize that the expressions obtained for ϕ_{BS} and σ_ϕ depend on only the properties of the neighborhood of z_0 because they are associated with the short time dynamics up to the Ehrenfest time. Nevertheless, later we will compute the inverse participation ratio of the intensities $|c_i|^2$, which depends on the long time dynamics up to the Heisenberg time, and then as we will show, a clear transition to quantum chaos will be appreciated.

To understand the mechanism associated with the avoided crossings we first notice that for a small perturbation, the separatrix divides the phase space into two regions where the motion is a rotation or a libra-

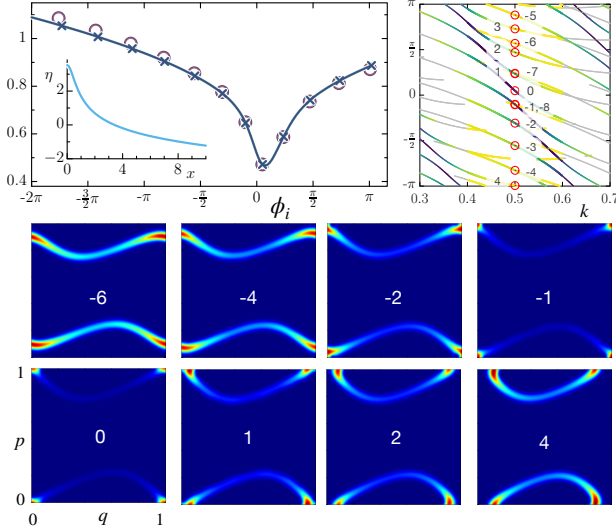


Figure 2. Manifestation of ESQPT in the eigenphase spectrum of the standard map. (Top left panel) Difference $\phi_{i+1} - \phi_i$ vs. ϕ_i for $k = 0.5$ and $N = 158$. Circles and crosses indicate quantum and semiclassical calculations, respectively. The inset shows $\eta(x)$ of Eq. (4). (Top right panel) Correlation diagram for $N = 158$ in the range $k = (0.3, 0.7)$. The thick colored lines represent $|c_i|^2 > 5 \times 10^{-6}$. (Bottom panels) Several eigenstates of the ESQPT in the Husimi representation.

tion, just like in a planar pendulum. Then, as we move adiabatically on an eigenphase with high intensity that passes through an avoided crossing, the corresponding eigenstate, previously localized on an invariant curve corresponding to rotation, transitions to an invariant curve that corresponds to libration [32].

Let us discuss the structure of eigenfunctions and eigenphases with the highest intensities $|c_i|^2$ at $k = 0.5$, a value of perturbation far from the breakup region (see Fig. 1). In the top right panel of Fig. 2 the eigenphases with the highest $|c_i|^2$ are marked with (red) circles, while in the top left panel we show the neighbor spacings $\phi_{i+1} - \phi_i$ vs. ϕ_i . These spacings have a minimum at ϕ_{BS} , with this bunching of levels being a characteristic feature for ESQPT; that is, quantum criticality is expressed by accumulation of levels around the separatrix [8]. To compute the spacings the phases need to be unfolded; that is, if ϕ_i is in a line coming from a previous (subsequent) Demkov structure, we add (subtract) 2π . The corresponding eigenfunctions are localized on invariant tori close to the separatrix; the bottom panels of Fig. 2 display the Husimi function [37] of these states. The state closest to the separatrix, labeled 0, is highly localized on the periodic point z_0 due to the dynamics on the separatrix. States labeled with positive integers are localized on tori with libration motion, and those labeled with negative integers are on tori with rotation motion.

Now we will obtain the previous result at a semiclassical level by using a technique based on the stable and unstable manifolds of z_0 (thick red and blue lines in Fig. 1).

The intersection of these manifolds defines the set of homoclinic orbits (HOs) of z_0 . Each HO consists of an infinite sequence of points that accumulate at z_0 . The main accomplishment of this theory is the ability to compute a semiclassical autocorrelation function of the wave packet centered on a PO, which is written as a sum over HOs, each one characterized by four canonical invariants (see [27, 32] for more details). Then, the Fourier transform of the autocorrelation function gives a smoothing of the spectral function $\Phi(\phi) = \sum |c_i|^2 \delta(\phi - \tilde{\phi}_i)$, expressed in terms of the product of two real functions $\tilde{F}(\phi)\Sigma(\phi)$ [32]. The function $\tilde{F}(\phi)$ is positive definite and describes the envelope of the intensities, with a maximum value at $\phi = \phi_{BS}$. As we are interested here only in the semiclassical determination of $\tilde{\phi}_i$, this function is not relevant for our analysis. In contrast, the function $\Sigma(\phi)$ is strongly oscillatory, and its maxima give us the eigenphases influenced by $|z_0\rangle$. This function is a sum over HOs, where each term is the product of an amplitude and the cosine of the phase [27]

$$\psi_j(\phi) = S_j/\hbar - \mu_j\pi/2 + x\eta(x) + x\ln(A_j/\hbar), \quad (4)$$

where $x = (\phi_{BS} - \phi)/\lambda$, S_j is the homoclinic action, μ_j the homoclinic Maslov index and A_j is the relevance. Moreover, $\eta(x)$ is a real even function with the only maximum at the origin (see the inset in the top left panel of Fig. 2 and further details in [32]). The evolution up to the Heisenberg time requires an enormous number of terms into the sum of $\Sigma(\phi)$. Nevertheless, we want to describe eigenfunctions localized on invariant curves close to the broken separatrix, which are well defined in terms of an evolution up to the Ehrenfest time. Therefore, only a few HOs are sufficient. Using a large number of HOs in this case does not provide new information and the only effect is to reduce the width of the smoothed delta functions defining the eigenphases. Furthermore, for small and moderated perturbations the amplitudes associated with the first two HOs are much greater than the next ones and consequently, we will restrict the analysis to these two. These amplitudes are very similar in the considered range of k ; e.g., the relative difference is 3.9×10^{-5} for $k = 0.5$ and goes to zero with k . Then to evaluate the maxima of $\Sigma(\phi)$ we include only the cosine factors $\Sigma(\phi) \propto \cos(\psi_1) + \cos(\psi_2)$. To compute this function we notice that the first HO is marked with circles in Fig. 1(e), and the second one is marked with triangles. The homoclinic Maslov indices are $\mu_1 = 0$ and $\mu_2 = 1$ for all k . For $k = 0.5$, $S = (S_1 + S_2)/2 \approx 0.142258$, $\Delta S = S_2 - S_1 \approx 1.2 \times 10^{-5}$, $A = (A_1 + A_2)/2 \approx 0.53998$ and $\Delta A = A_2 - A_1 \approx 5.8 \times 10^{-4}$.

We express $\cos(\psi_1) + \cos(\psi_2) = 2\cos(\psi)\cos(\Delta\psi/2)$, with $\psi = (\psi_1 + \psi_2)/2$ and $\Delta\psi = \psi_2 - \psi_1$. To leading order in the small quantity $\epsilon = \Delta A/A$ (ϵ goes to zero with k) we can consider $\Delta\psi = \Delta S/\hbar - \pi/2 + O(\epsilon)$ to be a constant (independent of ϕ). Hence, the maxima of the sum of cosines can be found (to leading order) with the quantization condition ($\cos\psi = 1$)

$$\psi = S/\hbar - \pi/4 + x\eta(x) + x\ln(A/\hbar) = 2\pi n. \quad (5)$$

This condition for finding the eigenphases that participate in the ESQPT is important because associates each solution with the quantum number n , an essential ingredient when the perturbation goes to zero. The integer providing the eigenphase with the smallest $|x|$ is $n_0 = 22$, corresponding to the one labeled 0 in Fig. 2, and the solution with $n = n_0 - l$ is the eigenphase labeled l . The top left panel of Fig. 2 shows that quantum and semiclassical calculations are very close. Furthermore, we have verified the accuracy of the eigenphases obtained from Eq. (5) for N up to 3000, finding an error $O(1/N)$. However, below we show that there is a critical value of N after which the validity of Eq. (5) no longer holds. Finally, we notice that an estimate of the mean nearest-neighbor spacing for the solutions of Eq. (5) is given by $\Delta\phi \sim \lambda/\ln(A/\hbar)$. Then, the number of eigenstates influenced by $|z_0\rangle$ results in $2\sigma_\phi/\Delta\phi \propto \ln(A/\hbar)$, and consequently the phenomenon of ESQPT introduces a logarithmic divergence for the mean density of states at ϕ_{BS} , in the semiclassical limit.

The quantization condition of Eq. (5) works over a wide range of perturbations up to $k \approx 1.1$, for the $N = 158$ case considered in Figs. 1 (central panel) and 2. Even though throughout this transition the chaotic region is (classically) growing, it is not large enough to be detected by quantum mechanics. This is evidence that the existence of classical chaos does not necessarily affect fine-size precursors. For larger k it is difficult to associate semiclassical solutions with quantum eigenphases, and for $k \approx 1.6$ the finite-size manifestation of ESQPT is destroyed. Due to the fact that this structure mainly depends on the first two HOs, it is expected that the destruction of the precursor of ESQPT happens when the contributions of these HOs cancel each other out. This criterion of strong perturbation occurs for $\cos(\Delta\psi/2) = 0$, or equivalently for $\Delta S/\hbar = 3\pi/2$. The functional dependence of ΔS on k allows us to define a perturbation value k_{break} where the ESQPT breaks up. Based on the definition of ΔS [see shaded area in Fig. 1(f)], we have obtained the following expression [32],

$$\Delta S(k) \approx 6\pi \left(1 - 0.341k^{1/3}\right) \exp\left(-\frac{\pi^2}{\sqrt{k}}\right), \quad (6)$$

with the exponential factor extracted from Ref. [38]. We observe that a characteristic of the breakup region is a sudden proliferation of contributing eigenphases. This effect is detected by a measure of localization of $|z_0\rangle$ in the basis $|\phi_i\rangle$ such as the inverse participation ratio $\xi = \sum |c_i|^4$. In Fig. 3 we show ξ/ξ_N , where ξ_N is a normalization factor so that $\xi/\xi_N = 1$ for $k \rightarrow 0$, as a function of the renormalized perturbation k/k_{break} for several values of N [32]. The evidence of full delocalization for $k/k_{\text{break}} \approx 1$ supports the accuracy of our ESQPT breakup estimation. In the inset of Fig. 3 we show k_{break} as a function of N which defines a phase diagram showing a region in which traces of ESQPT remain and a region where the precursors of criticality are fully destroyed. It can be clearly seen that k_{break} goes to zero in the semiclassical limit ($N \rightarrow \infty$).

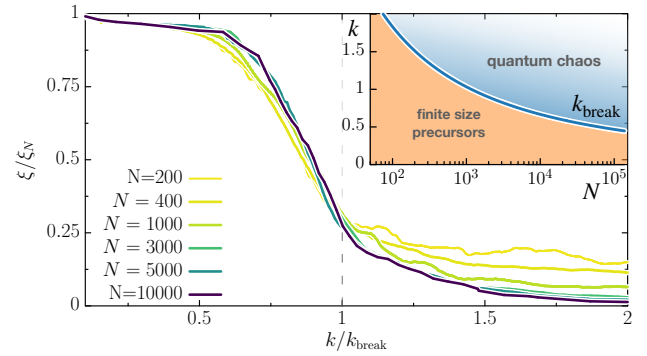


Figure 3. Normalized running average of the IPR of $|z_0\rangle$ vs. k/k_{break} for $N = 200, 400, 1000, 3000, 5000$, and 10000 . For all the curves a running average was performed to smooth out the fluctuations. Inset: k_{break} vs. N (see text for details). The normalization factor was empirically found to behave as $\xi_N \approx 3/(3.75 + \ln N)$.

Let us finally discuss qualitatively the transition process from localization to delocalization for $|z_0\rangle$. The top panel of Fig. 4 displays $|c_i|^2$ for $N = 158$ and $k = 1.447$ close to $k_{\text{break}}(158) \approx 1.62$, showing a much more complicated systematic than the intensities for $k = 0.5$ (shown in the inset). Intensities 1 and 2 are predicted for consecutive solutions of Eq. (5) with $n = 37$ and $n = 38$, respectively, while the associated states are reminiscent of states 0 and -1 in Fig. 2. The intensity labeled 3 approximately satisfies the equation $\psi_1 = 2\pi n_1$, with $n_1 = 38$, and state 3 shows a strong scar [27] of the PO, displayed with crosses; this PO is a satellite PO of the first HO [39]. Equivalently, intensity 4 verifies the equation $\psi_2 = 2\pi n_2$, with $n_2 = 39$, and state 4 shows a strong scar of the PO displayed with pluses, which is a satellite of the second HO. Finally, intensities 5 and 6 are not close to any of the three equations mentioned before, and both states exhibit characteristics of the three structures discussed in the previous panels. This description suggests that for k close to k_{break} , the phenomenon of scarring manifests clearly on satellite POs of the principal HOs, providing a signature of chaos at the quantum level. One observes a competition between two processes: coherent interference between HOs in order to generate ESQPT states and destructive interference between HOs giving rise to scars of satellites POs.

In summary, the effect of a perturbation on the finite-size precursors of ESQPTs was analyzed. We have demonstrated that the advent of chaos can decrease the quantum manifestations of an ESQPT whenever quantum mechanics is able to detect the small scale structures generated by chaos. In this sense classical chaos is a necessary but not sufficient condition to affect finite size precursors of ESQPT. We revealed that the mechanism of this phenomenon is the destructive interference between principal homoclinic orbits of the unstable periodic trajectory that generates criticality. Moreover, a semiclassical criterion specifying a transition to quantum chaos was established.

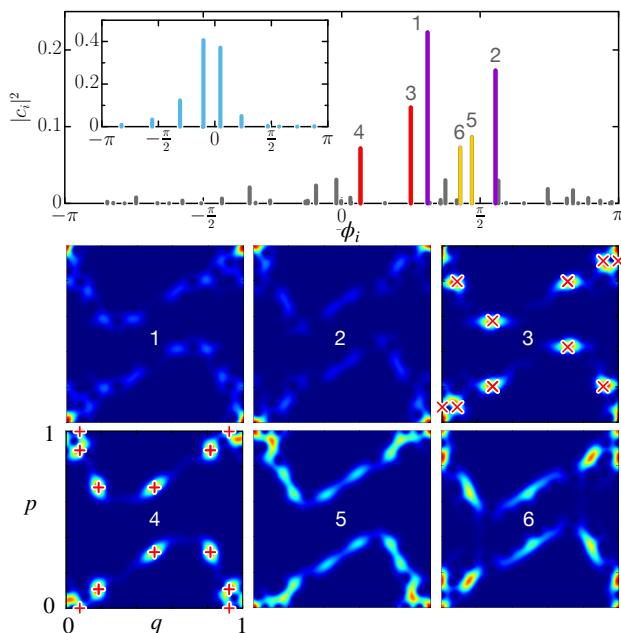


Figure 4. Top: Intensities $|c_i|^2$ of $|z_0\rangle$ for $k = 1.447$ and $N = 158$; the inset shows the case $k = 0.5$ and $N = 158$. Bottom: Husimi representation of eigenstates with high intensities. Panel 3) shows a satellite PO (crosses) of the first HO, and panel 4 shows a satellite PO (pluses) of the second HO.

Finally, we would like to emphasize the use of manifolds of unstable POs for the semiclassical description of a quantum perturbation. These Lagrangian manifolds, unlike tori, are structurally stable and for this reason are suitable for analyzing the effect of perturbations over the system.

We acknowledge the valuable discussions held with Juan Diego Urbina and Quirin Hummel. The work was partially supported by CONICET (PIP 112201 50100493CO), UBACyT (Grant No. 20020170100234BA), ANPCyT (PICT-2016-1056). I.G-M received support from the French-Argentinian project LIA-LICOQ.

-
- [1] P. Coleman and A. Schofield, “Quantum criticality,” *Nature* **433**, 226–229. (2005).
 - [2] S. Sachdev, *Quantum Phase Transitions* (Cambridge University Press, Cambridge, 1999).
 - [3] Pavel Cejnar, Pavel Stránský, Michal Macek, and Michal Kloc, “Excited-state quantum phase transitions,” *J. Phys. A: Math. Theo.* **54**, 133001 (2021).
 - [4] A. Relaño, J. M. Arias, J. Dukelsky, J. E. García-Ramos, and P. Pérez-Fernández, “Decoherence as a signature of an excited-state quantum phase transition,” *Phys. Rev. A* **78**, 060102 (2008).
 - [5] Qian Wang and Francisco Pérez-Bernal, “Excited-state quantum phase transition and the quantum-speed-limit time,” *Phys. Rev. A* **100**, 022118 (2019).
 - [6] Qian Wang and H. T. Quan, “Probing the excited-state quantum phase transition through statistics of loschmidt echo and quantum work,” *Phys. Rev. E* **96**, 032142 (2017).
 - [7] Qian Wang and Francisco Pérez-Bernal, “Characterizing the Lipkin-Meshkov-Glick model excited-state quantum phase transition using dynamical and statistical properties of the diagonal entropy,” *Phys. Rev. E* **103**, 032109 (2021).
 - [8] Quirin Hummel, Benjamin Geiger, Juan Diego Urbina, and Klaus Richter, “Reversible Quantum Information Spreading in Many-Body Systems near Criticality,” *Phys. Rev. Lett.* **123**, 2262 (2019).
 - [9] T Tian, H X Yang, L Y Qiu, H Y Liang, Y B Yang, Y Xu, and L M Duan, “Observation of Dynamical Quantum Phase Transitions with Correspondence in an Excited State Phase Diagram,” *Phys. Rev. Lett.* **124**, 043001 (2020).
 - [10] P. Feldmann, C. Klempt, A. Smerzi, L. Santos, and M. Gessner, “Interferometric Order Parameter for Excited-State Quantum Phase Transitions in Bose-Einstein Condensates,” *Phys. Rev. Lett.* **126**, 230602 (2021).
 - [11] V M Bastidas, G Engelhardt, P Pérez-Fernández, M Vogl, and T Brandes, “Critical quasienergy states in driven many-body systems,” *Phys. Rev. A* **90**, 063628 (2014).
 - [12] Victor Manuel Bastidas, Pedro Pérez-Fernández, Malte Vogl, and Tobias Brandes, “Quantum Criticality and Dynamical Instability in the Kicked-Top Model,” *Phys. Rev. Lett.* **112**, 140408 (2014).
 - [13] Jayendra N Bandyopadhyay and Tapomoy Guha Sarkar, “Effective time-independent analysis for quantum kicked systems,” *Phys. Rev. E* **91**, 032923 (2015).
 - [14] M. A. Lieberman (auth.) A. J. Lichtenberg, *Regular and Stochastic Motion*, 2nd ed., Applied Mathematical Sciences 38 (Springer New York, 1983).
 - [15] Michal Kloc, Pavel Stránský, and Pavel Cejnar, “Quantum quench dynamics in dicke superradiance models,” *Phys. Rev. A* **98**, 013836 (2018).
 - [16] Pavel Stránský, Michal Macek, and Pavel Cejnar, “Excited-state quantum phase transitions in systems with two degrees of freedom: Level density, level dynamics, thermal properties,” *Annals of Physics* **345**, 73–97 (2014).
 - [17] Pavel Stránský, Michal Macek, Amiram Leviatan, and Pavel Cejnar, “Excited-state quantum phase transitions in systems with two degrees of freedom: Ii. finite-size effects,” *Annals of Physics* **356**, 57–82 (2015).
 - [18] Michal Macek, Pavel Stránský, Amiram Leviatan, and Pavel Cejnar, “Excited-state quantum phase transitions

- in systems with two degrees of freedom. III. Interacting boson systems,” *Phys. Rev.C* **99**, 064323 (2019).
- [19] Michal Kloc, Pavel Stránský, and Pavel Cejnar, “Monodromy in dicke superradiance,” *J. Phys. A: Math. Theo.* **50**, 315205 (2017).
 - [20] Michal Kloc, Pavel Stránský, and Pavel Cejnar, “Quantum phases and entanglement properties of an extended dicke model,” *Annals of Physics* **382**, 85–111 (2017).
 - [21] Matthias Brack and Rajat Bhaduri, *Semiclassical Physics* (Addison-Wesley Publishing Company, Inc., 1997).
 - [22] M C Gutzwiller, *Chaos in Classical and Quantum Mechanics*, Interdisciplinary Applied Mathematics (Springer New York, 2013).
 - [23] I. C. Percival, “Chaos in hamiltonian systems,” *Proceedings of the Royal Society of London. A. Mathematical and Physical Sciences* **413**, 131–143 (1997).
 - [24] Eduardo G. Vergini, “Semiclassical approach to long time propagation in quantum chaos: Predicting scars,” *Phys. Rev. Lett.* **108**, 264101 (2012).
 - [25] Eduardo G. Vergini, “Semiclassical propagation up to the heisenberg time,” *EPL (Europhysics Letters)* **103**, 20003 (2013).
 - [26] Eduardo G Vergini, “Semiclassical theory of long time propagation in quantum chaos. first part,” *J. Phys. A: Math. Theo.* **53**, 395703 (2020).
 - [27] Eduardo G. Vergini, “Semiclassical quantization of highly excited scar states,” *EPL (Europhysics Letters)* **118**, 10005 (2017).
 - [28] D Wisniacki, E Vergini, R Benito, and F Borondo, “Signatures of Homoclinic Motion in Quantum Chaos,” *Phys. Rev. Lett.* **94** (2005).
 - [29] D A Wisniacki, E Vergini, R M Benito, and F Borondo, “Scarring by Homoclinic and Heteroclinic Orbits,” *Phys. Rev. Lett.* **97**, 094101 (2006).
 - [30] B. Chirikov and D. Shepelyansky, “Chirikov standard map,” *Scholarpedia* **3**, 3550 (2008), revision #194619.
 - [31] Eduardo G Vergini and Gabriel G Carlo, “Semiclassical construction of resonances with hyperbolic structure: the scar function,” *J. Phys. A: Math. Gen.* **34**, 4525–4552 (2001).
 - [32] See Supplemental Material..
 - [33] FJ Arranz, F Borondo, and RM Benito, “Avoided crossings, scars, and transition to chaos,” *The Journal of chemical physics* **107**, 2395–2406 (1997).
 - [34] Ji-Hwan Kim, Jaewon Kim, Chang-Hwan Yi, Hyeon-Hye Yu, Ji-Won Lee, and Chil-Min Kim, “Avoided level crossings in an elliptic billiard,” *Phys. Rev. E* **96**, 916 (2017).
 - [35] David Schneider Eduardo G Vergini and Alejandro M F Rivas, “The short periodic orbit approach for the quantum cat maps,” *J. Phys. A: Math. Theo.* **41**, 405102 (2008).
 - [36] F J Arranz, F Borondo, and R M Benito, “Scar Formation at the Edge of the Chaotic Region,” *Phys. Rev. Lett.* **80**, 944–947 (1998).
 - [37] Kōdi Husimi, “Some formal properties of the density matrix,” *Proceedings of the Physico-Mathematical Society of Japan. 3rd Series* **22**, 264–314 (1940).
 - [38] VF Lazutkin, IG Schachmannski, and MB Tabanov, “Splitting of separatrices for standard and semistandard mappings,” *Physica D: Nonlinear Phenomena* **40**, 235–248 (1989).
 - [39] Associated to each HO, there are an infinite set of unstable satellite POs which approximate more and more the motion of the HO as the period goes to infinity. Furthermore, the Bohr-Sommerfeld of these satellite POs is close to the quantization of the HO expressed by the relationship $\psi_j = 2\pi n..$

Supplemental material to “Impact of chaos on precursors of quantum criticality”

Appendix A: Adiabatic evolution of eigenstates in an ESQPT

In Fig. S1 we show the adiabatic evolution of an eigenstate when it goes through an ESQPT. In the top panel of S1, we plotted a region of the correlation diagram of Fig. 1 (of the main text) with eigenvalues ϕ_i that have overlap square $|c_i|^2 > 10^{-6}$. We have highlighted with red dots the adiabatic evolution of one of the eigenstates. In the bottom panels of Fig. S1, we show the Husimi function of the eigenstates marked in the top panel with the corresponding label. It can be clearly seen that before the non-isolated avoided crossing, the eigenstates are localized in tori of rotational motion (panels 1, 2 and 3). As we get closer to the middle of the avoided crossing, the state is located on the periodic orbit z_0 (panels 4 and 5) and then the eigenstates are located in tori of libration motion (panels 6, 7 and 8).

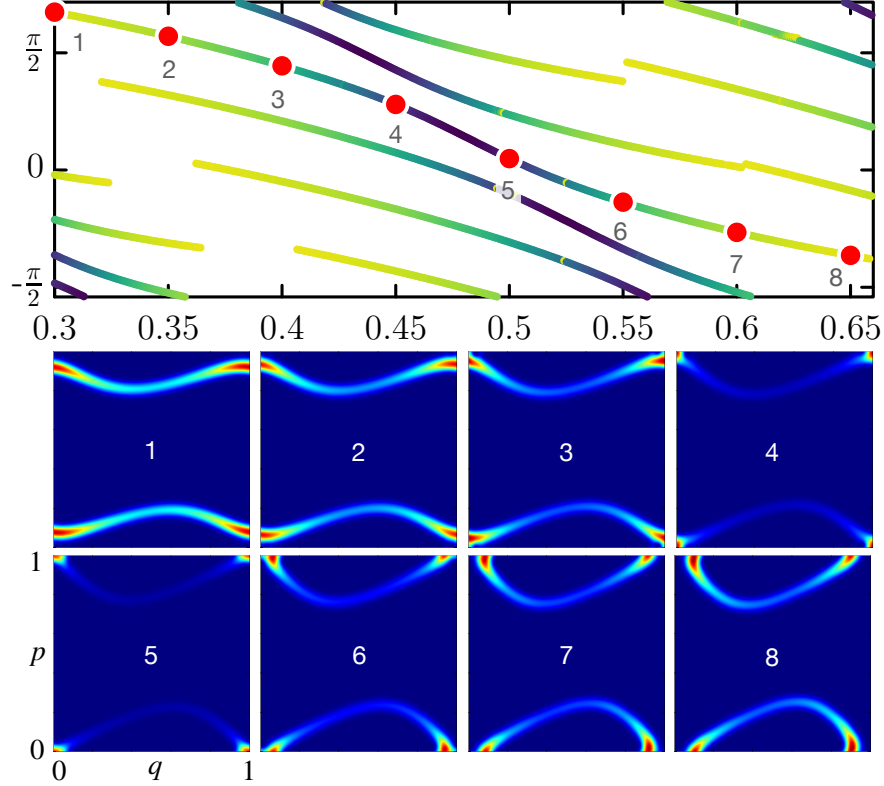


Figure S1. Top panel: A region of the correlation diagram of Fig. 1(main text) with overlap square $|c_i|^2 > 10^{-6}$ with the resonance of the PO $(q, p) = (0, 0)$. Bottom panel: Eigenstates adiabatically crossing an non-isolated avoided crossing marked in the top panel.

Appendix B: Resonance $|z_0\rangle$ of the fixed point z_0

A resonance of an unstable PO is a Gaussian beam constructed in the neighborhood of the PO; see equation (124) in [S26]. Here, such construction reduces to a wave packet centered at the fixed point $z_0 = (0, 0)$. We first write the wave packet in the plane $q - p$

$$W(q) = \left(\frac{\sinh \lambda}{\pi \hbar} \right)^{1/4} \exp \left[-\frac{q^2}{2\hbar} \left(\sinh \lambda + i \frac{k}{2} \right) \right]. \quad (\text{S1})$$

Later, one projects $W(q)$ on the unit torus

$$\langle j|z_0\rangle = W(j/N) + W(j/N - 1) \quad \text{for } j = 0, \dots, N - 1. \quad (\text{S2})$$

The mean value of the evolution operator in the state $|z_0\rangle$ can be estimated by the simple semiclassical expression

$$\langle z_0|\hat{U}|z_0\rangle \simeq \frac{e^{i\phi_{BS}}}{\sqrt{\cosh \lambda}}, \quad (\text{S3})$$

with the Bohr-Sommerfeld phase ϕ_{BS} being the action of the map at the fixed point z_0 , divided by \hbar .

Appendix C: Semiclassical smoothing of the spectral decomposition of $|z_0\rangle$

We rewrite equation (5) of reference [S27] for the case of an are-preserving map in the unit torus (we use the notation introduced in the letter)

$$\sum |c_i|^2 g\left(\frac{2(\phi - \tilde{\phi}_i)}{\lambda\beta}\right) \simeq K \tilde{F}(x) \left(1 + \frac{1}{\lambda\sqrt{N}} \sum \frac{\cos(\psi_j)}{\sqrt{A_j|L_j|}}\right), \quad (\text{S1})$$

where the sum runs over the set of HOs with relevance $A_j < A_{max}$, with $\beta = 2/\ln(2\pi N A_{max})$ and L_j the Lazutkin canonical invariant. Moreover, $K = \sqrt{\pi/8\beta/(1+\beta)}$ and

$$g(y) = \frac{\sin(y)/y + \beta \cos(y)}{(1 + \beta^2 y^2)(1 + \beta)} \quad \text{for } y \neq 0 \quad \text{and} \quad g(0) = 1. \quad (\text{S2})$$

As A_{max} increases, one has to include more HOs into the sum. Then the fuction $g(2(\phi - \tilde{\phi}_i)/\lambda\beta)$ is closer to a delta function and the eigenphases are better defined.

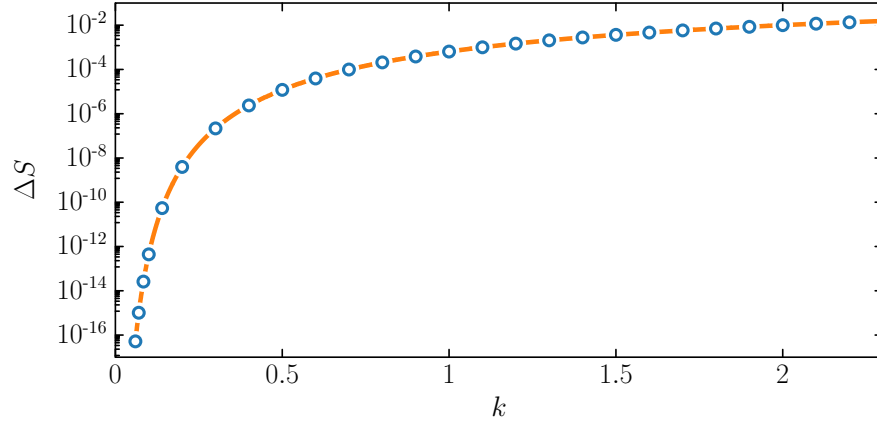


Figure S2. The points are the calculated values of ΔS and the solid line corresponds to the estimated function of Eq. (6) in the main text.

Appendix D: Approximation of ΔS

In Fig. S2 we show the estimation Eq. (6) (main text) of the canonical invariant $\Delta S = S_2 - S_1$ (black shaded area in Fig. 1(f)) as a function of k

Appendix E: The functions $\eta(x)$ and $\tilde{F}(x)$

The functions $\eta(x)$ and $\tilde{F}(x)$ are defined in terms of the Fourier transform of other functions [S27]. For this reason, in order to provide simple expressions here we present accurate interpolation formulas.

The function $\varphi(x) = x\eta(x)$ is the phase of the complex function

$$\tilde{f}(x) = \frac{1}{\sqrt{\pi}} \int_{-\infty}^{\infty} e^{-y/2} K_0(e^{-y}) e^{ixy} dy, \quad (\text{S1})$$

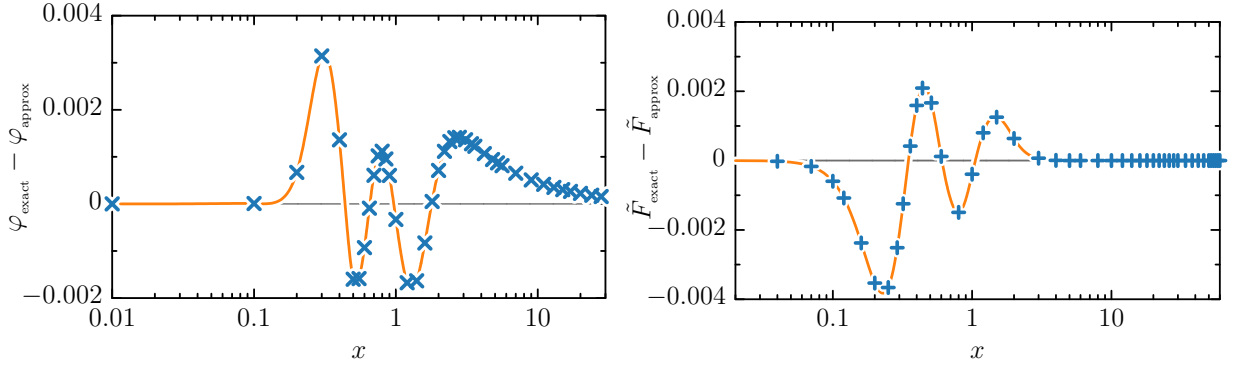


Figure S3. Error in the approximation of $\varphi(x)$ and $\tilde{F}(x)$.

with K_0 the modified Bessel function of zeroth order. That is $\tilde{f}(x) = |\tilde{f}(x)|e^{i\varphi(x)}$, where we have selected the branch of the phase satisfying $\varphi(0) = 0$. The function $\eta(x)$ verifies the following asymptotic behaviours for $x \rightarrow 0$ and $|x| \rightarrow \infty$

$$\eta(x) = \eta(0) - ax^2 + bx^4 + \mathcal{O}(x^6) \quad \text{and} \quad \eta(x) = -\ln|x| + 1 + \frac{\pi}{4|x|} + \mathcal{O}(1/x^2), \quad (\text{S2})$$

with $\eta(0) \approx 3.53430\,63528$, $a \approx 5.38865\,58307$ and $b \approx 12.80436\,182$. Later, we propose an interpolation formula satisfying the previous behaviours

$$\eta(x) \approx -\ln\sqrt{x^2 + 1/2a} + 1 + A(1 + Bx^4)^{-1/4} + C(1 + z_1x^6)^{z_2 \ln(z_3 + x^2)}, \quad (\text{S3})$$

with $z_1 = 423$, $z_2 = -0.4337$ and $z_3 = 1.78$ free parameters fitted to minimize the error of the approximation for $\varphi(x)$ in the intermediate region. In contrast, the constants A , B and C are related to $\eta(0)$, a and b as follows

$$B = \left[\frac{16}{\pi}(a^2 - b) \right]^{4/5} \approx 34.190, \quad (\text{S4})$$

$A = \pi B^{1/4}/4 \approx 1.8992$, and $C = \eta(0) - \ln\sqrt{2a} - A - 1 \approx -0.5536$.

The function $\tilde{F}(x)$ is defined by the integral equation

$$\tilde{F}(x) = \sqrt{\frac{2}{\pi}} \int_0^\infty \frac{\cos(xy)}{\sqrt{\cosh(y)}} dy, \quad (\text{S5})$$

with asymptotic behaviours for $x \rightarrow 0$ and $|x| \rightarrow \infty$

$$\tilde{F}(x) = \tilde{F}(0) - cx^2 + \mathcal{O}(x^4) \quad \text{and} \quad \tilde{F}(x) = \sqrt{\frac{2}{|x|}} e^{-\pi|x|/2} (1 + \mathcal{O}(1/x^2)), \quad (\text{S6})$$

with $\tilde{F}(0) \approx 2.09209\,92401$ and $c \approx 8.99462\,98154$. Later, we propose an interpolation formula satisfying the previous behaviors

$$\tilde{F}(x) \approx \frac{(D^2 + x^2)^{-1/4}}{\sqrt{\cosh(\pi x)}} + E(1 + z_4x^4)^{-\ln\sqrt{z_5 + x^2}}, \quad (\text{S7})$$

with $z_4 = 103$ and $z_5 = 1.8$ free parameters fitted to minimize the error of the approximation for $\tilde{F}(x)$ in the intermediate region. In contrast, the constants $D \approx 0.31247$ and $E \approx 0.30316$ were derived from the relationships $\tilde{F}(0) = E + 1/\sqrt{D}$ and $c = (1 + D^2\pi^2)/(4D^{5/2})$.

Figure S3 shows the error of the previous approximations.

Appendix F: Detailed phase space portrait for $k = 1.447$

The infinite family of satellite POs of a given HO approximate more and more the motion of the HO as the period of the PO goes to infinity. This family consists of unstable POs with Bohr-Sommerfeld phase well approximated by

the condition $\psi_j(\phi) = 2\pi n$, with $\psi_j(\phi)$ the phase of the given HO. We have found that the shortest satellite PO of the first HO generates a strong scar on the eigenstate number 3 of Fig. 3 (of the main text), and the shortest satellite PO of the second HO generates a strong scar on the eigenstate number 4. Fig. S4 shows clearly these satellite POs, and their strong correlation with the Hussimis of states 3 and 4.

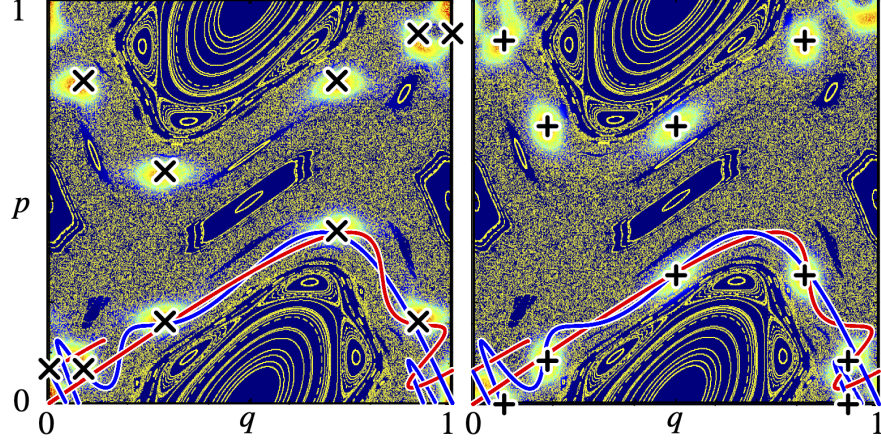


Figure S4. Eigenfunctions No. 3 and 4. from Fig. 3 of the main text, with the corresponding satellite orbit in black symbols and the unstable (solid red) and stable (solid blue) manifolds. The yellow dots represent the classical phase space for $k = 1.447$.

Appendix G: Scaling of the participation ratio with the system size

In Fig. 3 of the main text using a rescaling of the IPR ξ we could show that a transition effectively takes place at an estimated value k_{break} . For clarity, and completeness in Fig. S5 (left) we show a smoothing of the data obtained for ξ (with no normalization) as a function of the (unrescaled) perturbation k , for several values of N . We observe that as N grows, the step in the curves become steeper (and for smaller k). In fact, the – correspondingly colored – dots mark the k_{break} value, where a clear displacement is observed, as it was shown in the inset of Fig. 3 [main text].

A complementary view of the IPR is provided by its inverse, i.e. the participation ratio or participation number (PR). It is usually associated with the area of Hilbert space occupied. If the system is fully chaotic then this saturates to a constant value proportional to N .

In our case, the area filled by the chaotic layer is much smaller than unity (the area of the phase space) in the considered range of k . One should use an effective size $N_{\text{effective}}$ instead of N , with $N_{\text{effective}} \approx NA_{\text{chaotic}}$, and where A_{chaotic} is the classical area of the chaotic layer which depends on k . An elementary estimation, for small k , gives $A_{\text{chaotic}} \propto \Delta S/\lambda$, where ΔS is the area of each lobe (as represented in Fig. 1f), and $1/\lambda$ proportional to the number of lobes along the broken separatrix. To clarify this point, in Fig. S5 (right) we show PR/N as a function of k for a wide range of values of N . It can be clearly observed that for small k values the scaling of PR/N collapses onto the curve $\alpha\Delta S/\lambda$ (where α is a fitting prefactor). Furthermore, we observe that the PR of all the curves saturates at $N_{\text{effective}}$ in accordance with our previous prediction. On the other hand, in the small k limit $A_{\text{chaotic}} < \xi_N$ (where ξ_N is the normalization used in Fig. 3), and so we have $PR/N \sim \xi_N/N$.

Appendix H: Complementary data

In this section we present data that supports the discussion presented in the main text. In Fig. S6 we show the logarithmic singularity in the level spacings characteristic of the ESQPT, for a larger $N = 1026$ value and the same perturbation $k = 0.5$ as shown in Fig. 2 of the main text. The spectrum considered corresponds to the largest overlaps of the initial state $|z_0\rangle$ with the eigenstates of the map U . To compute the phase differences $\Delta\phi = \phi_{i+1} - \phi_i$, an unfolding procedure is necessary to account for contributions from different Demkov structures (see Fig. 2, main text). We note that the semiclassical calculation improves appreciably. This is expected because for $k \ll k_{\text{break}}$ the error is of order $1/N$. For the perturbation value considered here we can estimate, by solving for $N = 3/(4\Delta S)$ that the characteristic (singular) structure will break at $N \approx 62900$.

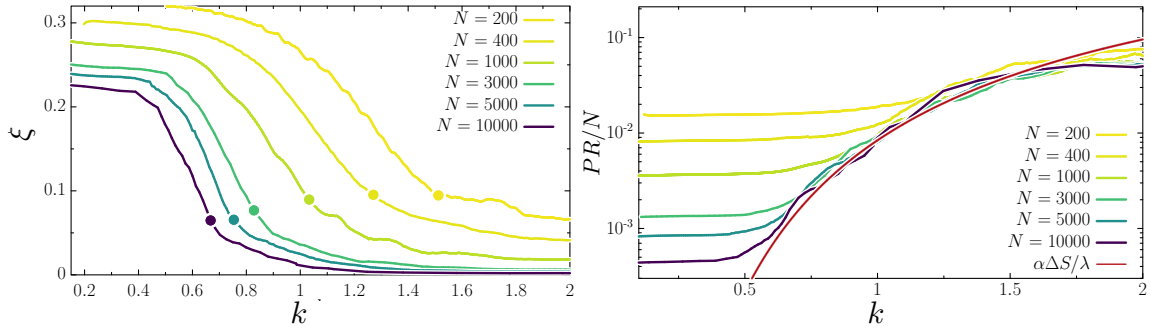


Figure S5. (Left) Smoothed IPR ξ as a function of k for $N = 200, 400, 1000, 3000, 5000, 10000$ (darkest shade is larger N). The dots correspond to the value of k_{break} obtained from $\Delta S / \hbar = 3\pi/2$ [see main text]. (Right) PR/N as a function of k for $N = 200, 400, 1000, 3000, 5000, 10000$ (darker color means larger N). The red line represents $\alpha \Delta S / \lambda$ (we took $\alpha = 14$). For all the curves a running average was performed to smooth out the fluctuations.

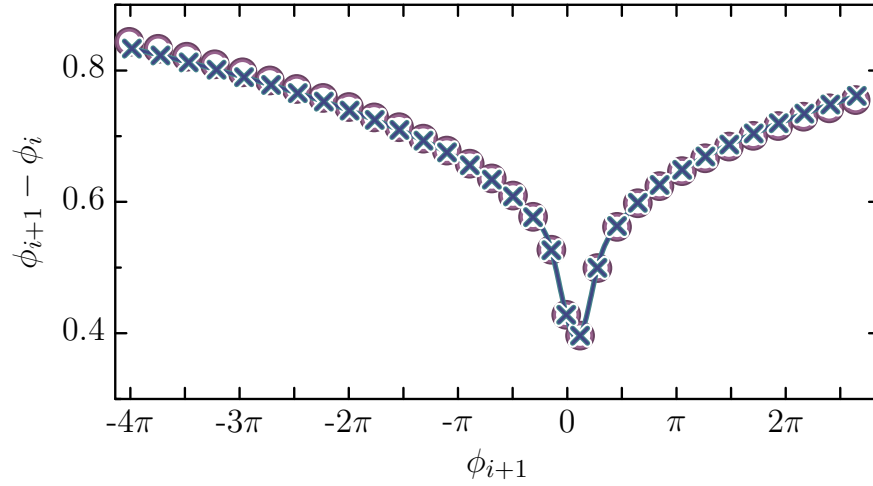


Figure S6. Level spacing singularity characteristic of ESQPT, for the standard map with $N = 1026$, $k = 0.5$. Circles and crosses indicate quantum and semiclassical calculation, respectively. The solid line is a cubic spline interpolation of the semiclassical calculation.